Application of Scanning Acoustic Microscopy to Polymeric Materials

F. LISY,[1] A. HILTNER,[1,*] E. BAER,[1] J. L. KATZ,[2] and A. MEUNIER[3]

[1]Department of Macromolecular Science and [2]Department of Biomedical Engineering, Case Western Reserve University, Cleveland, Ohio 44106; [3]Laboratoire De Recherches Orthopediques, URA CNRS 1432, Faculte De Medecine Lariboisiere Saint Louis, 10 Avenue De Verdun, 75010 Paris, France

SYNOPSIS

Scanning acoustic microscopy (SAM) is now a viable technique for the nondestructive evaluation of various materials. SAM is capable of distinguishing defects and discontinuities and/or the variations in elastic properties on a scale comparable to optical microscopy. The pulse mode utilizes a single narrow acoustic wave that permits surface and internal studies over a range of frequencies from 5 to 200 MHz with resolution down to approximately 20 μm. This technique was applied to image surface features of an opaque sheet-molding compound and to analyze flow patterns of chopped glass fibers. The pulse mode was also used to image the internal damage sustained from a high-speed projectile in oriented polypropylene and two carbon fiber-reinforced composites, with different matrices. Most importantly, the pulse mode of the acoustic microscope is a nondestructive method and the interior of samples that are entirely opaque can be readily studied with this unique instrument. The burst mode is composed of a group of acoustic waves and is capable of operating at higher frequencies than the pulse mode up to several gigahertz. This mode permits resolution down to the micrometer level and is especially useful for investigating surface and subsurface microstructural features. The burst mode was used to determine the distribution of chopped fibers in a PEEK matrix and carbon black particulates in an adhesive, the orientation of the mineral phase and density variations in a single osteon from a dog femur, and the orientation of collagen fibers in a sheep meniscus. Also, the sensitivity of the burst mode to surface features was used to examine the topographical features in a multilayer composite and a blend of poly(vinyl chloride) (PVC) with poly(ethylene terephthalate) (PET) particulates.

INTRODUCTION

Acoustic wave propagation, which is dependent on the velocity of sound, is primarily a function of both the density and elastic properties of a material. Also, the amplitude of an acoustic wave propagating in a medium is affected by numerous solid-state features. For this reason, analytical techniques based on acoustic wave propagation to evaluate, nondestructively, the internal integrity and the elastic properties of materials have intrigued investigators for many years. Ultrasonic techniques, such as the C-scan, using low-frequency acoustic signals are commonly used to find defects of greater than 1 mm inside solid materials. These methods are based on the propagation of plane longitudinal and/or shear waves.

The first step toward the nondestructive evaluation of the interior of a structure using acoustic microscopy was the scanning laser acoustic microscope (SLAM).[1] The SLAM used planar longitudinal acoustic waves. A significant breakthrough concerning lateral resolution was achieved by Lemons and Quate, who used an acoustic transducer that spherically focused the acoustic waves.[2] Later, they developed the first scanning version of an acoustic microscope that nondestructively examined the in-

* To whom correspondence should be addressed.

Journal of Applied Polymer Science, Vol. 52, 329–352 (1994)
 CCC 0021-8995/94/020329-24

terior of optically opaque materials on a scale comparable to light microscopy.[3] Today, most commercially available scanning acoustic microscopes (SAM) either operate in the burst or the pulse mode. A comprehensive review of the theories as well as many applications of scanning acoustic microscopy is provided in a recently published book by Briggs.[4]

The pulse mode, which operates in the low-frequency range (10–200 MHz), is composed of a single acoustic wave or pulse that permits in-depth imaging of internal defects and discontinuities. The low-frequency range limits the resolving power of the microscope (20–150 μm resolution in water). However, the relatively low resolution of this operating mode may be counterbalanced by the ability to penetrate deeper into the material and to scan over a larger area. Commonly, the pulse mode shows the delaminations in composites[5] or internal damage, inclusions, or voids in various materials.[4,6] Acoustic microscopes in the pulse mode can discriminate explicit echoes caused by the surface or by various internal structural defects.

The burst mode, which operates with higher frequencies (100–2000 MHz), permits much greater resolutions (down to 1 μm) at the expense of the depth of penetration. This mode is based on the propagation of groups of longitudinal acoustic wave bursts. Therefore, the burst mode is used to investigate surface and subsurface features of a material. The burst mode evaluates the characteristics of a material through examining either acoustic signals reflected directly from the surface or from their interferences with various surface (or subsurface) waves. The burst mode is highly sensitive to changes in local acoustic velocities.

A SAM in the burst mode was used to study the distribution and the orientation of SiC fibers in an aluminum matrix.[7] The acoustic microscope imaged the SiC fibers at both the surface and 10 μm below the surface with high contrast due to the much higher modulus of the fibers as compared to the aluminum matrix. Another application of the burst mode is to nondestructively investigate the grain structure of polycrystalline metals[8,9] and ceramics.[7] Since the burst mode can image differences in elasticity, the anisotropy in grains is well suited for this type of analysis without using an etchant or heat treating the specimen to cause topographical changes at the grain boundaries. Acoustic microscopy in the burst mode can even detect the change in properties of a metal associated with plastic deformation.[10] The region of plastic deformation was observable with acoustic waves since the velocity of sound changed by several percent in this region with respect to the matrix. Cracks are also imaged with the acoustic microscope working in the burst mode since this mode of operation involves the interferences from the surface waves and the waves reflected from the discontinuity.[11–14]

The purpose of this article was to show the applicability of SAM to polymeric materials and their composites and to give several examples of both the pulse and burst modes. The pulse mode will be used to investigate internal defects, whereas the burst mode will analyze variations in surface and subsurface features.

TECHNICAL BACKGROUND

The essential component in acoustic microscopy is the acoustic transducer, which is composed of a sapphire rod with a concave spherical surface at one end and an epitaxially grown piezoelectric transducer on its parallel surface (Fig. 1). When this transducer receives an RF signal from the transmitter, the RF signal is converted into plane acoustic waves that propagate through the rod. The concave surface of the transducer converges the acoustic signal to a single focal point. Acoustic microscopy requires a coupling medium (usually water) to transfer the focused, acoustic wave from the transducer to the specimen. The velocity of the acoustic wave in the sapphire rod is much higher than in the coupling liquid. Due to the high refractive index difference between the transducer and the coupling liquid, spherical aberration is negligible.

Presently, mechanical scanning of the transducer or the specimen is controlled by a computer, depending on the acoustic microscope and its operating mode. To obtain an image, the focal point is scanned over the specimen in the x-direction and then rastered in the y-direction. The acoustic wave at each point is reflected back to the transducer, which now acts as a receiver and transforms the reflected acoustic wave back into an RF signal. Then, an A/D converter translates the electrical voltage corresponding to the amplitude measurement into a digital value that is stored in the memory of a computer. This value is determined by the local acoustic characteristic of the specimen in a confined area, which size corresponds to the diameter of the focal point of the transducer. When the mapping is completed, the acoustic properties of the specimen are assigned a gray level for a selected range of amplitudes and displayed as luminous information on a monitor.

When investigating the amplitude of the main

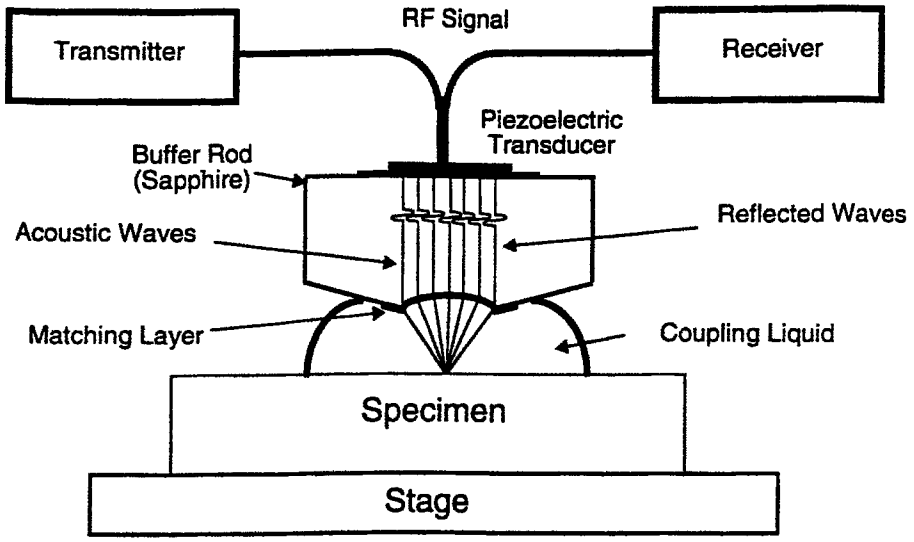

Figure 1 A schematic of a scanning acoustic microscope transducer (lens). The primary constituents of the transducer are the sapphire buffer rod with a conical surface at one end and a ZnO piezoelectric transducer on the other surface. A coupling liquid is used to transport the acoustic signals from the transducer to the specimen.

reflective signal, the acoustic characteristic of importance is the acoustic impedance (z):

$$z = \rho \times V_i$$

where ρ is the material density, and V_i, the velocity of the longitudinal acoustic wave propagating in the direction i (perpendicular to the surface). The difference between the acoustic impedance in the material and that of the coupling liquid is called the reflection coefficient (r), which is related to the acoustic impedances of the liquid couplant (Z_1) and the material (Z_2) through the following equation:

$$r = \frac{Z_2 - Z_1}{Z_2 + Z_1}$$

It is this parameter that determines the amplitude of the digital value stored in the computer. The principal features of the two main operating modes of a scanning acoustic microscope will now be reviewed.

Pulse Mode

The pulse operating mode is specifically suited for in-depth examination of materials (up to several millimeters). The input signal is a single narrow pulse and the returning signal is generally a succession of echoes, shown schematically in Figure 2. After the input signal reaches the surface, a part of the sound wave is reflected back, producing surface echoes. The remaining part of the input signal propagates through the specimen until it interacts with any interface in the interior that will reflect the signal and create secondary echoes. These echoes reach the transducer after a specific time depending on their depth and the sound velocity of the matrix material. The amplitudes of the reflected and transmitted waves are a function of the acoustic properties of the material at each point along the x-direction. An interface corresponds to any type of discontinuity in the local acoustic properties such as defects (cracks, voids, or delaminations) or real changes in properties (inclusions, laminated or fibrous material, or crystalline structure).

Another attraction of the pulse mode technique is illustrated in Figure 2(B). The pulse mode implements an adjustable time-delay gate that is used to isolate a chosen echo (or echoes) since the returning acoustic signal varies with depth of penetration of the input signal. Therefore, the delay gate is used to investigate the reflected signals from a specific region or discontinuity. Another technique to investigate the reflected signals from within a sample is called X–Z imaging, which is schematically shown in Figure 3. Initially, the focal point of the transducer is formed above the sample, which reduces the acoustic signal and shifts the signal to the right. The reflected signals are shifted to the right since they have a longer travel time from the sample

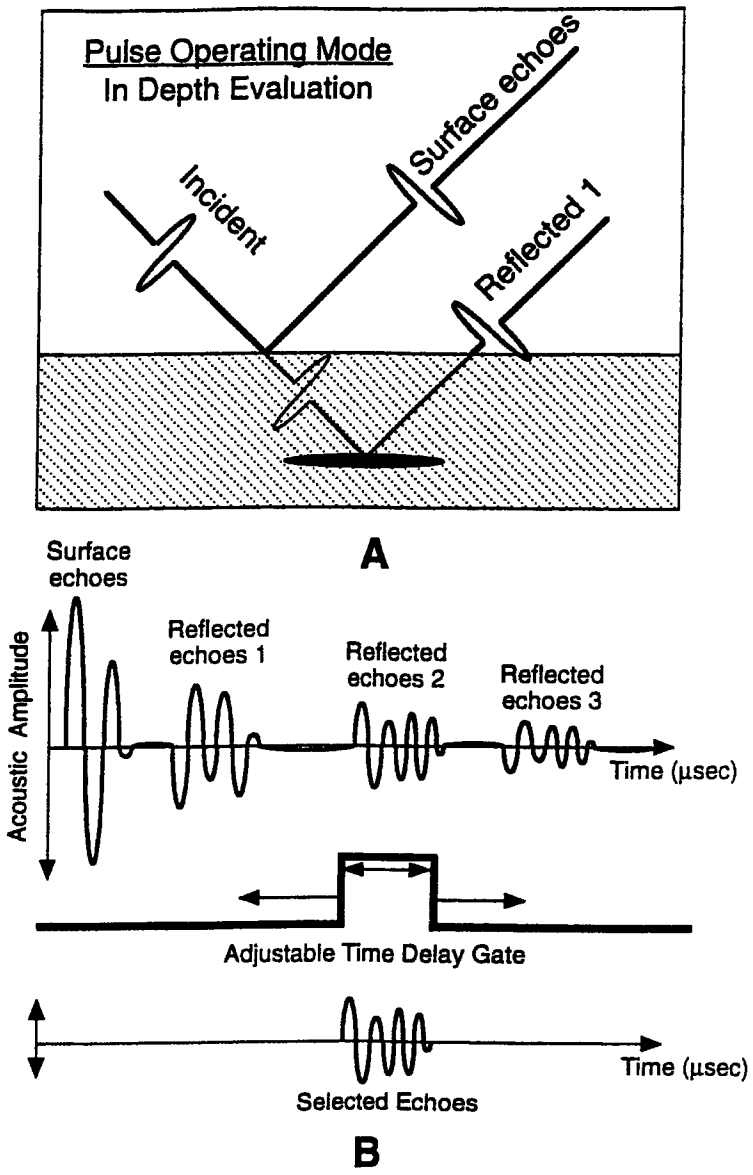

Figure 2 A schematic of the acoustic waves in the pulse mode. (A) shows the input signal of the pulse mode as a single acoustic wave that is partially reflected from the surface of the specimen and any internal discontinuities. (B) shows a schematic representation of the entire reflected signal and an adjustable delay gate that isolates specific reflected echoes.

back to the transducer. Next, the delay gate is placed to the left of these reflected signals. When the transducer is scanned in the x-direction and lowered, the reflected signals shift to the left as the travel time from the surface to the transducer is decreased. Therefore, the entire reflected signals must pass through the stationary delay gate and form the X-Z image.

The depth of imaging of the pulse mode may be several millimeters if a lower frequency transducer is used or the material has low attenuation of sound (less rigid material). However, the frequency of the acoustic wave is also proportional to the resolution of the acoustic microscope. For example, a low-frequency transducer will permit deep penetration of the acoustic wave at the expense of the resolution, whereas the high-frequency transducer will resolve smaller defects but not as deep in the material as will a low-frequency transducer. Therefore, pulse mode imaging requires an understanding of the acoustic properties of a material and its possible defects.

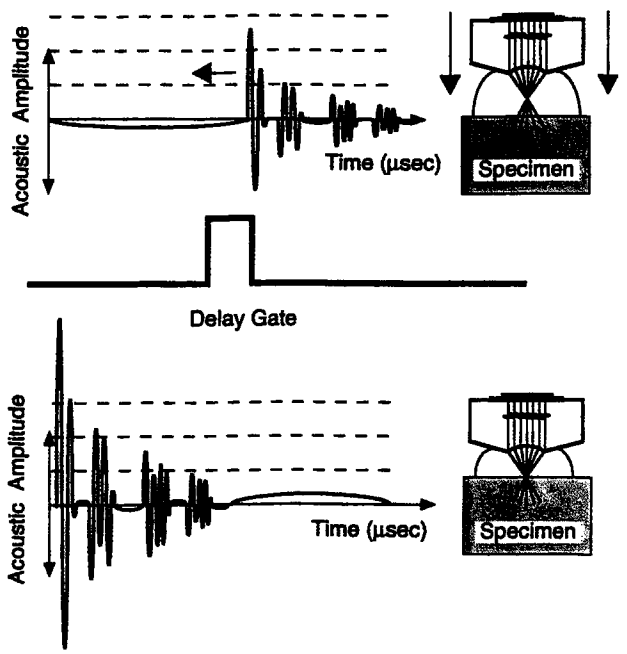

Figure 3 A schematic of how the reflected signal is collected to form an X-Z image in the pulse mode. The acoustic transducer is focused on the surface of the specimen and raised a certain distance, shifting the entire reflected signal to the right. Next, the transducer is mechanically scanned in the x-direction and lowered in the z-direction, which causes the reflected signal to move through the delay gate. The entire reflected signal is collected by the delay gate forming the X-Z image.

The depth of penetration of acoustic waves into a material is inversely proportional to the density and acoustic velocity of the material. Thus, polymers are a most suitable subject for SAM studies in the pulse mode.[4] The low acoustic impedance of polymers enables a greater proportion of the acoustic waves to be transmitted through the surface into the bulk, making internal imaging easier. Hence, the pulse mode transducer is ideal for most polymers. For low acoustic impedance materials such as polymers and soft biological tissues, a small change in z results in a large variation in the reflection coefficient, leading to a highly contrasted image. On the contrary, for materials exhibiting a very large z, such as ceramics or high-impedance metallic alloys, even a large change in z related to density or elastic property variations results in a minute change in the coefficient of reflection.

Burst Operating Mode

The alternative operating mode of the SAM known as the burst mode operates in the high-frequency range (from 100 MHz up to several GHz), which allows a much higher resolution. At the higher frequencies, absorption and dispersion become predominant; therefore, only surface or subsurface images can be obtained. Operation of the burst mode is very similar to that of the pulse mode. However, the burst mode uses an acoustic wave made of several (tens of) sinusoidal cycles rather than a single pulse as shown in Figure 4. Variations of the acoustic signal result from either (A) the intrinsic reflectivity of the material surface or (B) through interferences occurring between different surface and subsurface reflected signals.

Similar to isolating the first group of echoes in the pulse mode, the burst mode can be used to investigate acoustic reflectivity variations in materials through local changes in acoustic impedance. When the aperture angle of the transducer is larger than a critical angle, the transmitted acoustic signal can simultaneously generate both longitudinal and surface acoustic waves (Rayleigh waves). However, the surface acoustic waves (SAW) are more predominant with highly reflective materials. To utilize the longitudinal and surface acoustic waves, the transducer is defocused, i.e., focal point is positioned some distance z below the surface of the specimen. Thus, the longitudinal and surface waves interfere, producing an acoustic signal variation that is specific to the investigated material.

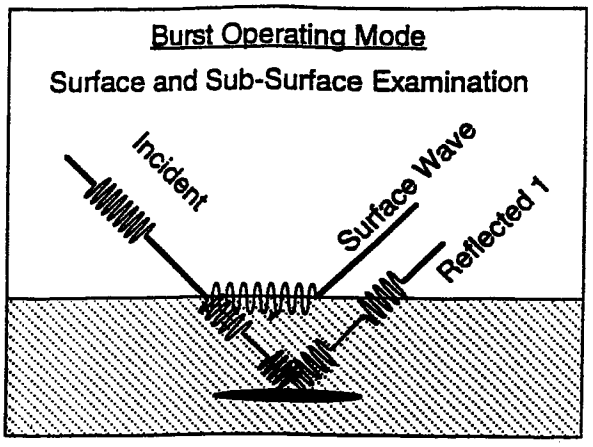

Figure 4 A schematic of the burst operating mode of the scanning acoustic microscope. A group of higher-frequency acoustic waves interacts with the surface and subsurface region of a specimen. The transducer collects either the surface echoes or the interferences from both the surface acoustic waves and the reflected echoes from subsurface discontinuities. Hence, subsurface acoustic images are a compilation of the surface acoustic waves and the reflected signal.

When the transducer is continuously defocused along the vertical axis, the result yields a trace called the $V(z)$ curve (Fig. 5). The $V(z)$ curve is a plot of voltage as a function of the location of the focal point below the surface. At $z = 0$, the focal point is at the surface of the specimen where the amplitude of the voltage signal is maximum. A $V(z)$ curve is directly related to the velocity of the surface acoustic wave. Therefore, materials with similar properties show negligible differences in acoustic amplitude when the transducer is focused on the surface. When the transducer is defocused (focal point is lowered below the surface), the differences in amplitude between the two $V(z)$ curves from various substructures found in a material create the contrast in the burst mode image. Since these substructures have different elastic properties, the interference patterns between longitudinal and surface waves vary according to the difference in elastic properties. Thus, acoustic images reveal these substructures provided that the transducer is properly defocused. This technique is used to investigate metallic alloys or ceramic structures and inclusions.

In most polymers, Rayleigh waves either do not propagate or require a critical angle not attainable even with large aperture angle transducers. For this reason, $V(z)$ curves are usually not used in the study of polymeric materials. A notable exception are polymers of high acoustic velocities (such as PMMA) in which another type of surface waves (surface skimming compressive waves [SSCW]) can propagate at the liquid/surface interface and produce interference patterns with the reflected signals similar to these obtained with Rayleigh waves.

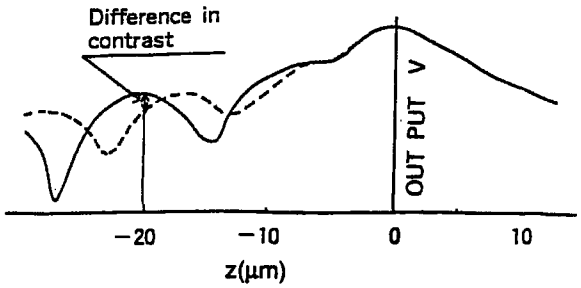

Figure 5 A schematic of two $V(z)$ curves (solid and dashed lines) from an anisotropic material. The $V(z)$ curve is a plot of voltage as a function of the location of the focal point. Materials with similar properties show negligible differences in the acoustic amplitude when the transducer is focused on the surface. When the transducer is lowered, the $V(z)$ curves show a variation in the velocity of the surface acoustic wave, thus obtaining a difference in contrast. (The schematic is courtesy of the Olympus Corp., with permission.)

The most common burst mode technique applied to polymeric materials generates an image from surface or subsurface interfaces resulting from a change in moduli. In the case of a second phase (such as a reinforcing material) or a defect, an image is formed from the interference patterns occurring between the burst signal reflected from both the surface and the subsurface interface. However, the burst mode is not capable of imaging subtle differences with respect to domain structures in a homogeneous matrix, on the micron level. Due to the large scattering and absorption of acoustic waves at high frequencies, the burst mode cannot provide images very deep below the surface, no greater than 500 microns in polymers.

EXPERIMENTAL

Materials

The pulse mode is especially suited for studying internal defects in a material; hence, three samples that absorbed internal damage differently were investigated. The first impacted sample was a commercial grade of polypropylene from Cadillac Plastics, which was biaxially oriented by cold rolling. The cold-rolling process reduced the thickness of the plaque to 80% of its original thickness, which, in essence, flattened the polypropylene spherulites parallel to the surface. A carbon fiber-reinforced PEEK composite was supplied by NASA Lewis Research Center. This composite had a 90, 0, 45 symmetrical layup. The third impacted sample was an intricately woven carbon fiber-reinforced epoxy composite supplied by the 3M Co. The carbon bundles in this sample were much larger than the bundles in the PEEK composite. Therefore, the damage caused by the impact was expected to propagate differently in these two carbon fiber-reinforced composites. The pulse mode was also used to determine the orientation of glass fibers in a sheet-molding compound (SMC) provided by Premix Corp. composed of a vinyl ester resin reinforced with chopped fibers.

The burst mode was used to investigate materials that exhibited differences in microscopic surface and subsurface features. A PEEK matrix reinforced with chopped carbon fibers was studied. Two elastomeric adhesives containing carbon black supplied by

Tremco Inc. with varying process histories were analyzed to elucidate the dispersion of the carbon black particles. The burst mode was also used to investigate the differences in orientation in the cortical region of a dog femur and in fresh sheep meniscus. The topography of two materials under strain was also studied using the burst mode. The topography of polished cross sections of a multilayer composite supplied by the Dow Chemical Co. and of a poly(vinyl chloride) (PVC)/poly(ethylene terephthalate) (PET) blend supplied by B. F. Goodrich was examined.

Sample Examination

All the samples were investigated with the UH3 scanning acoustic microscope made by the Olympus Corp. The UH3 can operate in both the burst and pulse modes. The pulse mode required the specimen to be placed in a tank of water below the transducer to couple the acoustic transducer to the sample, while the burst mode utilized a drop of water. The frequency of the transducer varied according to the material and the information being obtained. In all cases, the samples required a relatively flat surface (low radius of curvature) and minimal surface roughness.

Since the area scanned by the pulse mode is much larger than that of the burst mode (due to the size of the focal point), the pulse mode is much more sensitive to the curvature of the sample. In the burst mode, which operates at higher frequencies than the pulse mode, surface roughness is a major concern. The effect of surface roughness varies with the frequency of the transducer since the wavelength of the acoustic waves at the higher frequencies is more likely to interfere with the smaller defects on the surface.

Impacted samples were investigated with the pulse mode transducer. The samples, confined at their ends, were impacted with a spherical 3.2 mm stainless-steel projectile traveling at 150 ft per s. However, the surfaces of the samples did not require preparation before the impact. The SMC sample was machined so that the section of interest, which had a slightly curved surface, could be studied. Hence, the curved surface was noted in the interpretation of the pulse mode image.

The burst mode samples varied in the amount of preparation required for scanning acoustic microscopy, and in most cases, the samples did not require any preparation for analysis. These samples had a surface finish comparable to a surface polished with 1 μm Al_2O_3 powder. The elastomeric adhesives reinforced with carbon black were cast onto glass plates that formed an ideal flat surface for acoustic microscopy. The multilayer composite and the PET-filled PVC samples were polished with 1 μm Al_2O_3 powder to remove larger surface defects. Then, the samples were mounted in a minideformation stage attached to the SAM and strained for SAM burst mode examination.

The dog femur required polishing with 0.3 μm Al_2O_3 powder. However, this specimen needed to be mounted and dried so that additional back-scattered electron microscopy for purposes of comparison could be performed in a low-voltage JEOL 840A scanning electron microscope. Biomaterials do not have to be mounted for acoustic microscopy since the liquid couplant prevents the biomaterials from degrading.

RESULTS AND DISCUSSION

Pulse Mode

Impact Damage in Oriented Polypropylene

Researchers at CWRU have improved the strength and toughness of polypropylene using a solid-state rolling process that gives similar properties to a hydrostatic extrusion method.[15] The polypropylene plaque was biaxially oriented in a cold-rolling mill that reduced the plaque to 20% of its original thickness. The impact damage was examined with the 30 MHz pulse mode transducer from both the impacted side and the back side of the sample, as shown in Figure 6. The 30 MHz transducer was chosen over the 100 MHz transducer since the 100 MHz transducer was not able to collect the echoes from the lower discontinuity from the impacted side of the sample. The first three 30 MHz images were formed from the impacted side of the sample. The surface echoes [Fig. 6(A)] show the indent from the impact on the surface of the sample along with two scratches. This image is very similar to the optical microscope image of the surface. The acoustic images formed from the discontinuities below the surface show that the internal damage from the projectile was somewhat parallel to the surface of the sample [Fig. 6(B) and (C)]. Hence, the impact appears to have caused the polypropylene to delaminate in the thickness direction, i.e., perpendicular to the direction of the impact.

The acoustic image in Figure 6(C) depicts an el-

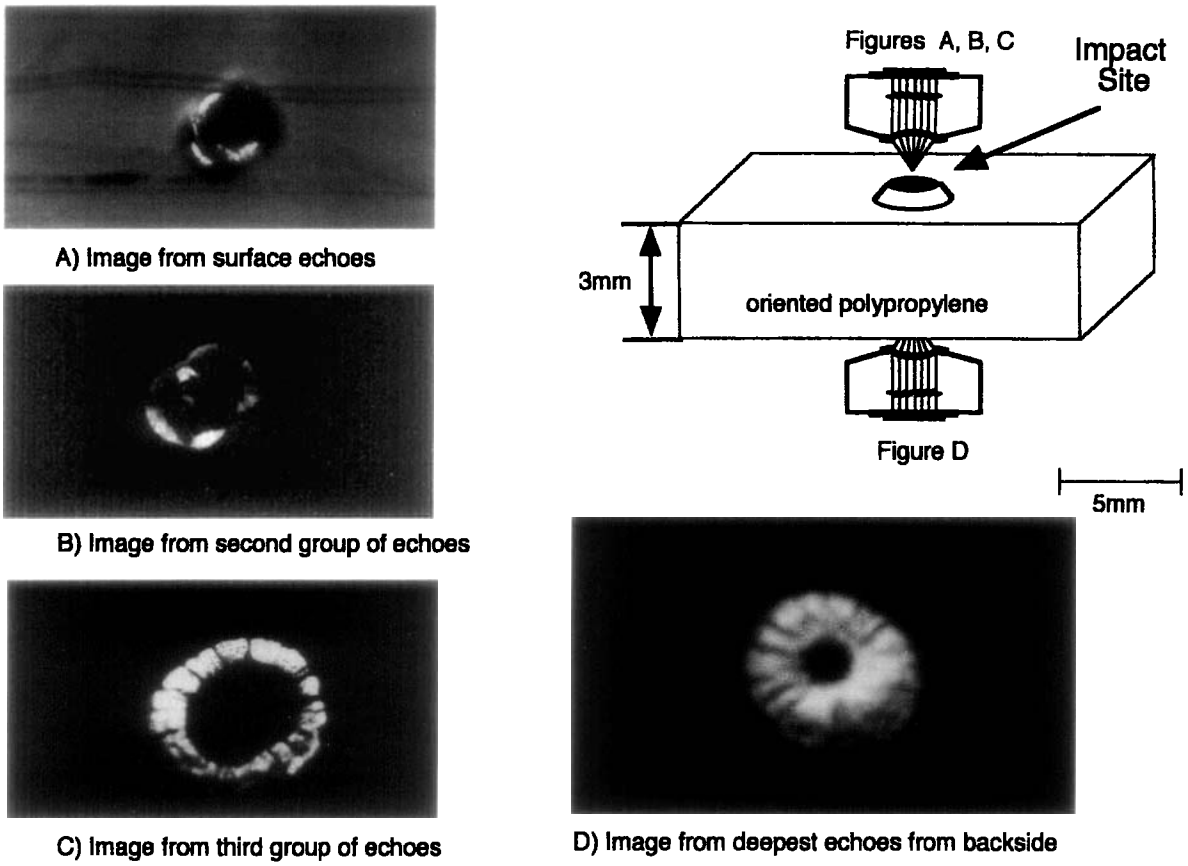

Figure 6 Scanning acoustic images from the 30 MHz pulse mode transducer of oriented polypropylene after it was impacted. (A–C) are acoustic images collected from the impacted side: from the surface, second group, and third group of echoes, respectively. (D) is the acoustic image from the back side of the impacted sample.

liptical ring-shaped discontinuity. However, the discontinuity may have been a solid ellipse since the signal may have been prevented from transmitting to the center portion of the ellipse due to the discontinuity shown in Figure 6(B) that is closer to the surface. To determine if the void in the center of the ellipse existed, the sample was inverted and the 30 MHz pulse mode transducer was used to image the defect from the back surface [Fig. 6(D)]. The low impedance of acoustic signals in the polypropylene allowed the defect to be imaged, though it was approximately 3 mm away from the back surface. The pulse mode image from the back surface shows a complete ellipse, which verifies that the damage caused by the impact was a couple of solid ellipses (one above the other) rather than a ring emanating from the above discontinuity.

To study the source of reflectance of the acoustic signal and the depth of the discontinuities, *X–Z* images were created. Two separate *X–Z* images were taken: one at position A and the other at position B, as indicated on the pulse mode image that shows both the second and third group of echoes [Fig. 7(A)]. The *X–Z* images were taken in the middle of the impact site [Fig. 7(B)] and near the edge of the impact as shown in Figure 7(C). One should be cautious with the interpretation of *X–Z* images. Generally, no echoes will return to the transducer from beneath a large discontinuity, since most or all of the acoustic waves are reflected back to the transducer from the discontinuity closest to the transducer. It appears that the first discontinuity prevented any acoustic waves from penetrating and imaging deeper into the oriented polypropylene. Therefore, the outer edges of a lower discontinuity are the only features of a deeper layer of delamination. The *X–Z* images depict a damage zone underneath the surface with a slight curvature away from the impact. Optical microscopy permits a two-dimensional view of the damage as compared to a three-dimensional representation from the acoustic images. Most importantly, the acoustic microscope

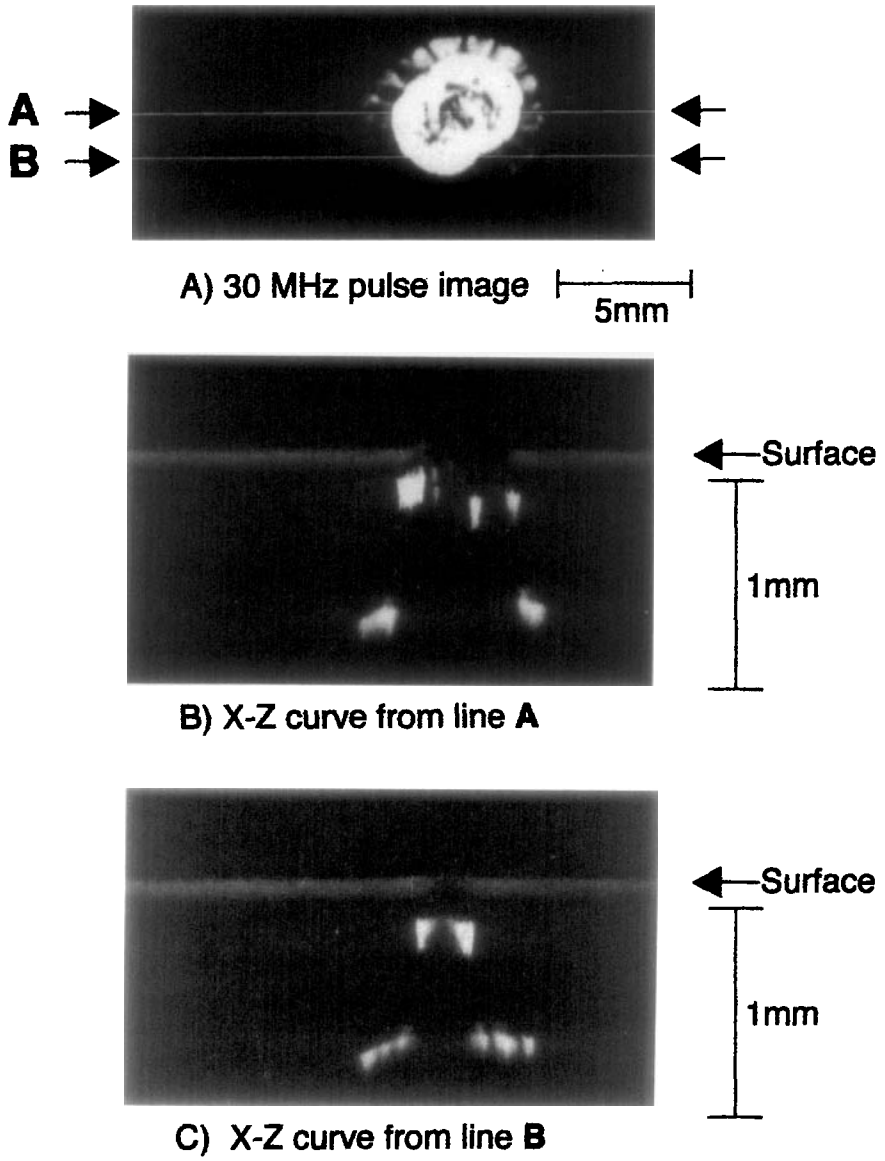

Figure 7 The *X–Z* images from the impacted polypropylene shown in Figure 6. (A) shows the acoustic image from the second and third groups of echoes and the location of both *X–Z* scans. (B,C) show the *X–Z* images from the center of the defect and slightly below the defect, respectively.

is a nondestructive method and information can be obtained from entirely opaque samples.

Impact Damage in Carbon Fiber-reinforced PEEK Composites

The polymeric composites reinforced with carbon fibers exhibit a very high stiffness-to-weight ratio. Therefore, these materials are ideal for aeronautical and space structural applications. However, the impact properties of these materials are of concern since the adhesion between the polymer matrix and the fibers may be compromised after an impact. In the area of impact, the acoustic microscope was used to investigate the structural integrity of a carbon fiber-reinforced PEEK composite after it was subjected to several impacts. The surface of the composite displayed several indents that indicated the impact sites of the projectiles. Optically, the composite displayed minimal surface damage and the opacity of the material limited the use of optical microscopy. It is in such a case where SAM be-

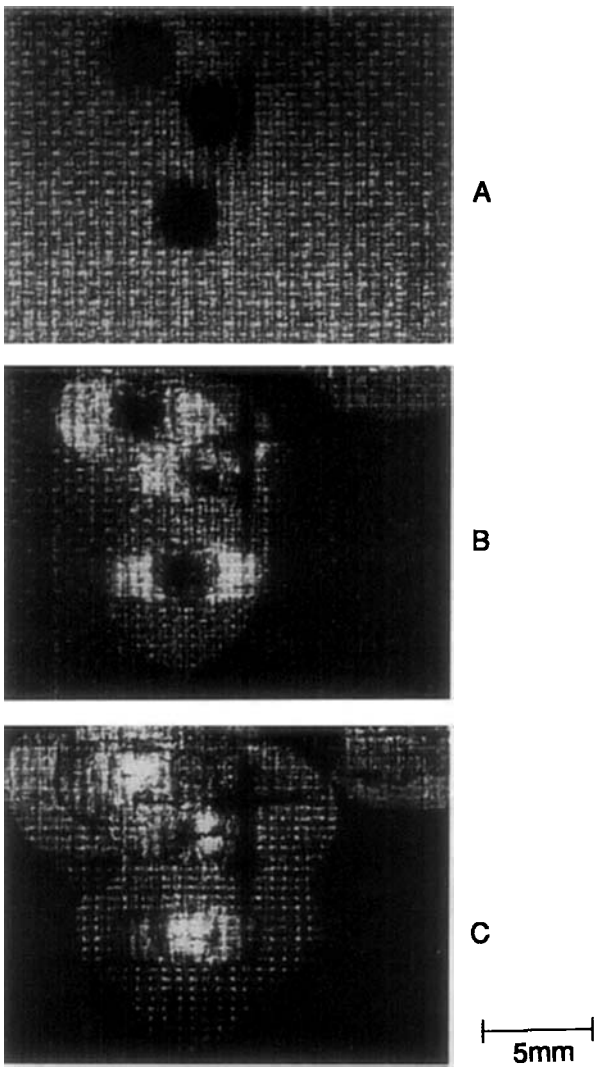

Figure 8 Three 30 MHz pulse mode acoustic images of a carbon fiber-reinforced PEEK composite impacted several times. The acoustic images were formed from groups of acoustic signals reflected off the (A) surface, (B) first, and (C) second discontinuities within the composite.

comes the nondestructive technique of choice. For this material, the 100 MHz pulse transducer displayed several layers of internal damage, as shown in Figure 8.

Figure 8(A) shows the SAM image produced from the surface echoes of the composite. This image shows recessed regions caused by three individual impacts. The SAM image of the surface is similar to what would be observed through optical microscopy. Figure 8(B) and (C) was created by isolating groups of echoes reflected from successively deeper discontinuities. The delay gate of the pulse mode was used to isolate these groups of echoes. In Figure 8(B) and (C), the delamination associated with the three central impacts coalesced. Interestingly, the delamination associated with another impact is also observed in the upper right portion of both Figure 8(B) and (C).

An X–Z image was obtained along a line through one of the impacts on the composite as shown in Figure 9(A). The X–Z image [Fig. 9(B)] shows the relative location and depth of the acoustic echoes beneath the surface. The X–Z image also shows the echoes that were isolated for all three pulse mode images in Figure 8. The X–Z image shows the regions at which the attenuation was manually decreased as the transducer was lowered toward the surface. Therefore, the horizontal and linear changes in contrast are artifacts of manually lowering the attenuations during X–Z imaging. If the attenuation was not manually lowered, the surface echoes would not be scaled in relation to the internal echoes; hence, the surface echoes would be very bright, making the damage indistinguishable. Even though reducing the attenuations manually left an artifact on the X–Z image, the damage pattern is still clear, emanating from the impact site. The depths of the discontinuities shown in Figure 8(B) and (C) as determined by the X–Z image were approximately 0.2 to 0.7 and 0.7 to 1.5 mm below the surface, respectively.

Damage in Woven Fiber-reinforced Composite

To improve the impact properties of composite materials, intricate weaving patterns connect the fiber bundles together. One such woven composite provided by the 3M Co. consists of an epoxy matrix with carbon fiber bundles. The composite was impacted as described above with a high-speed projectile. In this impact study, the weave of the composite was larger, which will also influence the internal damage as investigated with the pulse mode. Optically, the woven composite surface displayed minimal damage caused by the projectile. The 30 MHz pulse transducer located several regions below the surface where the structural integrity was compromised. The 30 MHz transducer was used on this woven composite since the larger carbon fiber bundles prevented the 100 MHz acoustic signal from penetrating into the composite. The larger weave of the composite also changed the characteristics of the impact damage, as previously observed in the PEEK composite described above.

Figure 10(A) shows the SAM image produced from the echoes reflected from the surface of the

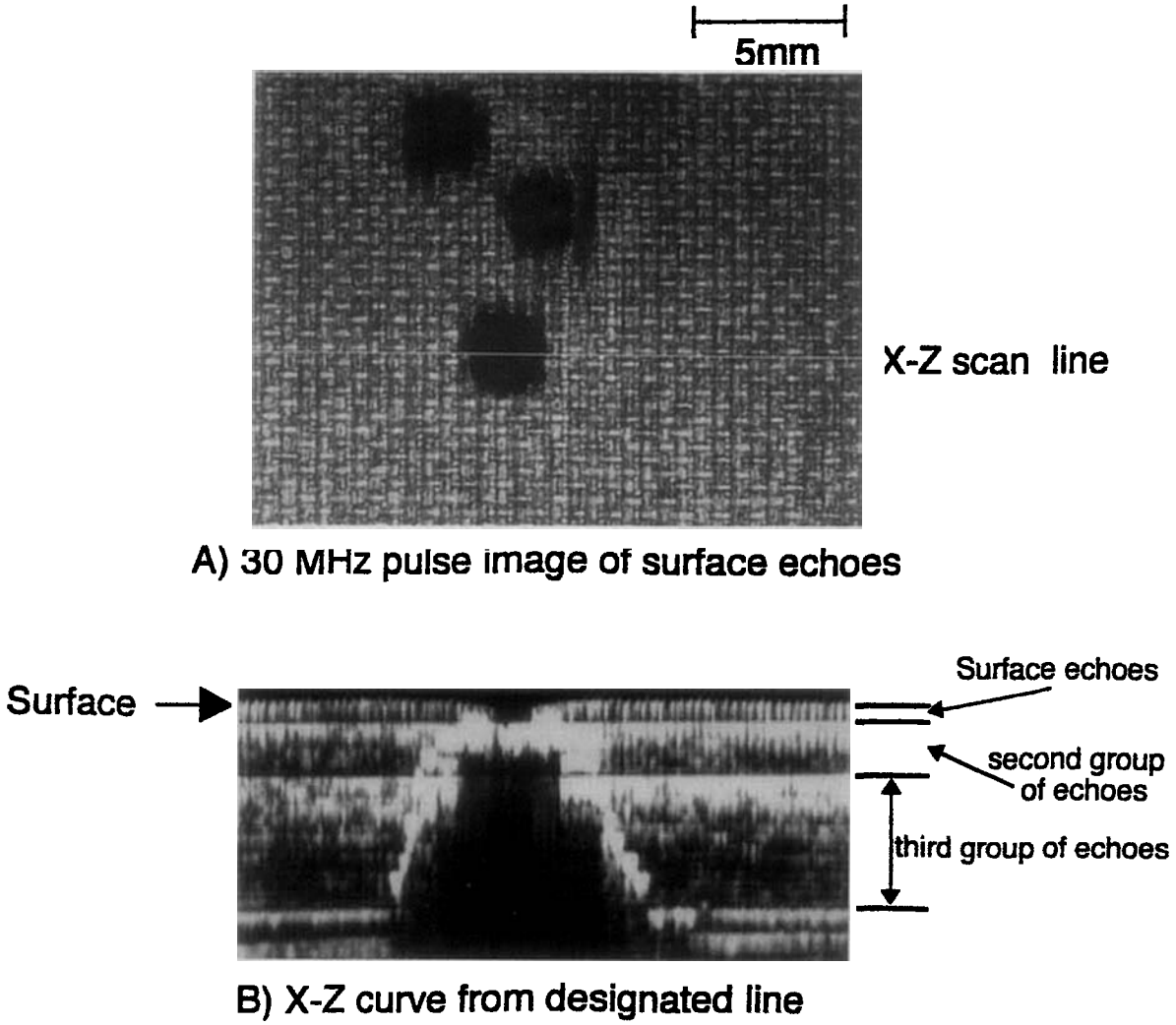

Figure 9 The acoustic image from the surface echoes of the impacted carbon fiber-reinforced PEEK composite. (A) shows the region where the *X–Z* curve was scanned. The *X–Z* image (B) shows the regions at which the attenuation was manually decreased as the transducer was lowered toward the surface. Hence, the horizontal and linear changes in contrast are artifacts of manually lowering the attenuations during *X–Z* imaging. The damage pattern is still very clear emanating from the impact site.

composite. This pulse mode image distinctly displays the weave and a single impact site on the surface of the composite. Figure 10(B) and (C) shows internal damage at successively deeper depths into the composite. Figure 10(B) shows a damaged region approximately 0.3–0.6 mm below the surface that interfered with the signal obtained from a depth of 0.6 to 1.2 mm [Fig. 10(C)]. To verify the shape and trajectory of the damage into the composite, an *X–Z* image was obtained through the impact site [Fig. 11(A)]. The *X–Z* image in Figure 11(B) revealed a recessed region from the impact on the surface and the underlying discontinuities which reflected the acoustic signal. The damage propagated downward into the matrix along carbon bundles. In this case, the damage appeared to propagate at an angle starting at the impact site and broadening as the depth increased. The exact size of the damage zone observed in the third acoustic image could not be determined since part of the acoustic signal was reflected by the interfaces or discontinuities before reaching that depth. It is obvious the impact damage was not layers of delamination between plies of carbon fibers as observed in the previous example since the impact damage propagated along the larger carbon fiber bundles that connected the layers together.

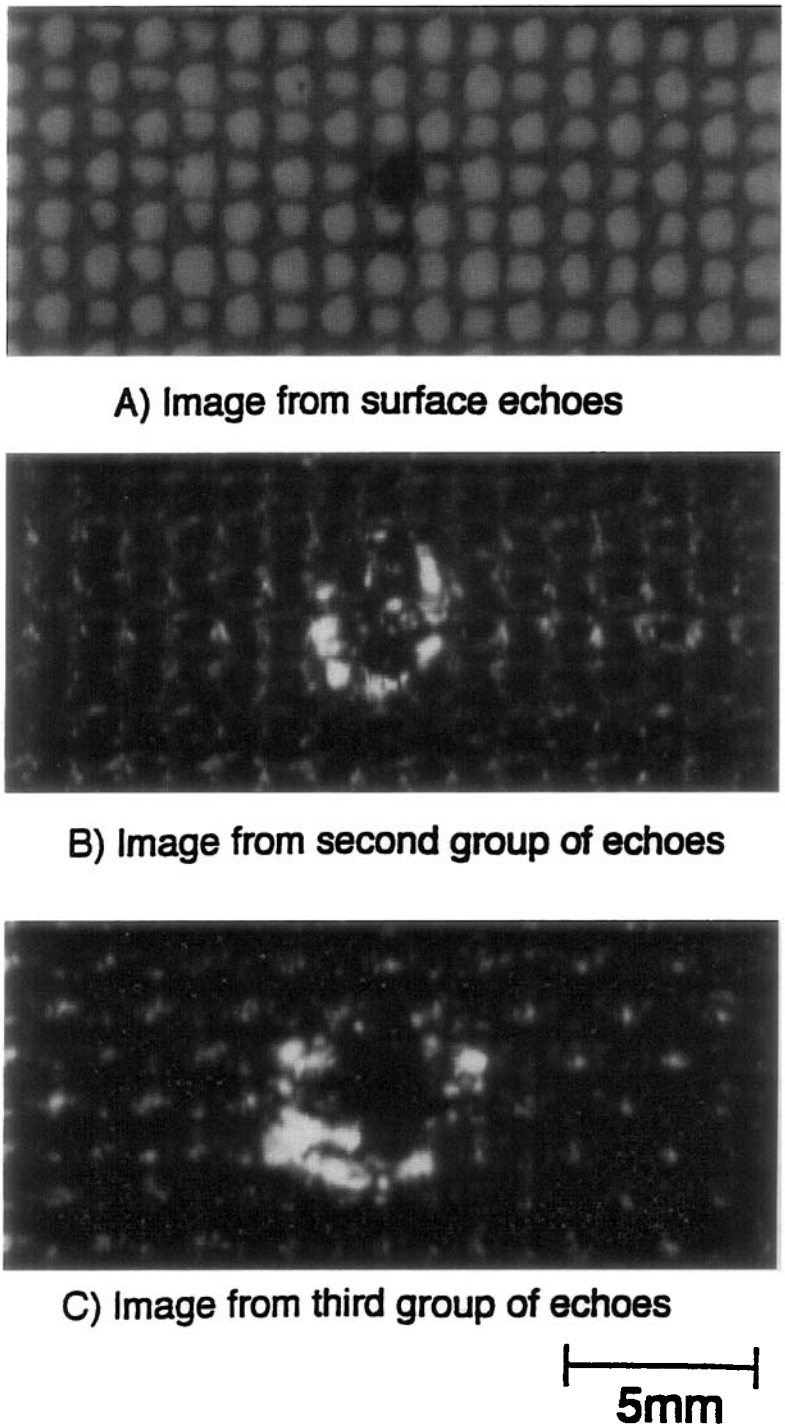

Figure 10 Three 30 MHz pulse mode images of a woven graphite fiber-reinforced epoxy composite impacted with a single high-speed projectile. (A–C) are from the surface, second group, and third groups of echoes, respectively.

Flow Fronts in a Sheet-molding Compound

A sheet-molding compound (SMC) is expected to flow and cure in a heated die to a desired intricate shape. Proper flow through the die is crucial for the structural integrity of the final product. However, the complexity of the die can inhibit proper flow of the SMC in certain regions forming internal defects

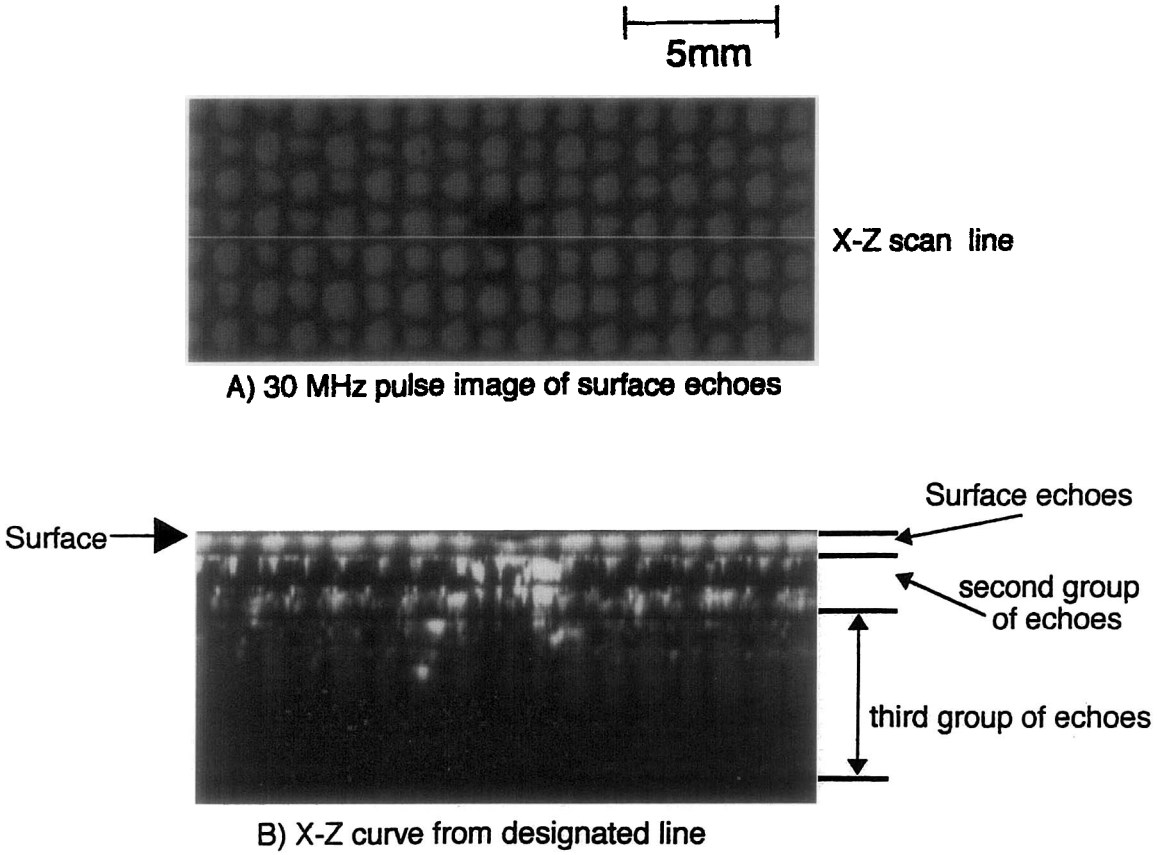

Figure 11 *X–Z* image from an impacted woven graphite fiber-reinforced epoxy composite. (A) shows the SAM image from the first group of echoes and the location of the *X–Z* scan. (B) shows the *X–Z* image, which shows the relative location of the acoustic signals beneath the impact.

in the mold. Therefore, an understanding of the flow patterns of the SMC and an evaluation of the structural integrity is necessary. The SMC was opaque, preventing any conventional optical microscopy examination of the flow patterns or the detection of any internal flaws. By using a 30 MHz pulse mode transducer, it was possible to nondestructively view the interior of the sample and evaluate the flow patterns to detect regions where the structural integrity might be compromised. A 100 MHz transducer was also used to investigate the orientation of the glass fibers along the surface of the mold. The higher-frequency transducer had a much higher resolution of the surface features but limited depth penetration.

Figure 12 shows a SAM image of oriented glass fibers in a molding that had good structural integrity. A comparison can be made with Figure 13, which shows the SAM image of a molding with an inferior flow pattern. The distribution of chopped glass fibers observed from the surface echoes [Figs. 12(A) and 13(A)] is similar using the 30 MHz transducer. To obtain a higher-resolution image of the glass fiber orientation, the 100 MHz transducer was used (Fig. 14). Figure 14(A) and (B) is from both the good and inferior moldings, respectively. The 100 MHz images show much more detail than the respective 30 MHz counterparts. In Figure 14, the inferior molding shows fewer glass fibers in the defect region as compared to the good mold. Even in Figure 14(B), the internal defect is visible since it is just below the surface. However, the 100 MHz transducer is not capable of a detailed evaluation of the interior since the signal is almost completely reflected from the surface.

The 30 MHz transducer was used to create images from the second and third groups of echoes to show the glass fiber orientation in the molding from approximately 0.3 to 0.7 and 0.7 to 1.6 mm below the surface, respectively. Figure 13(B) and (C) revealed the flow fronts of the SMC at these two levels as well as the defect in the molding with an improper flow front. The large dark regions in these acoustic

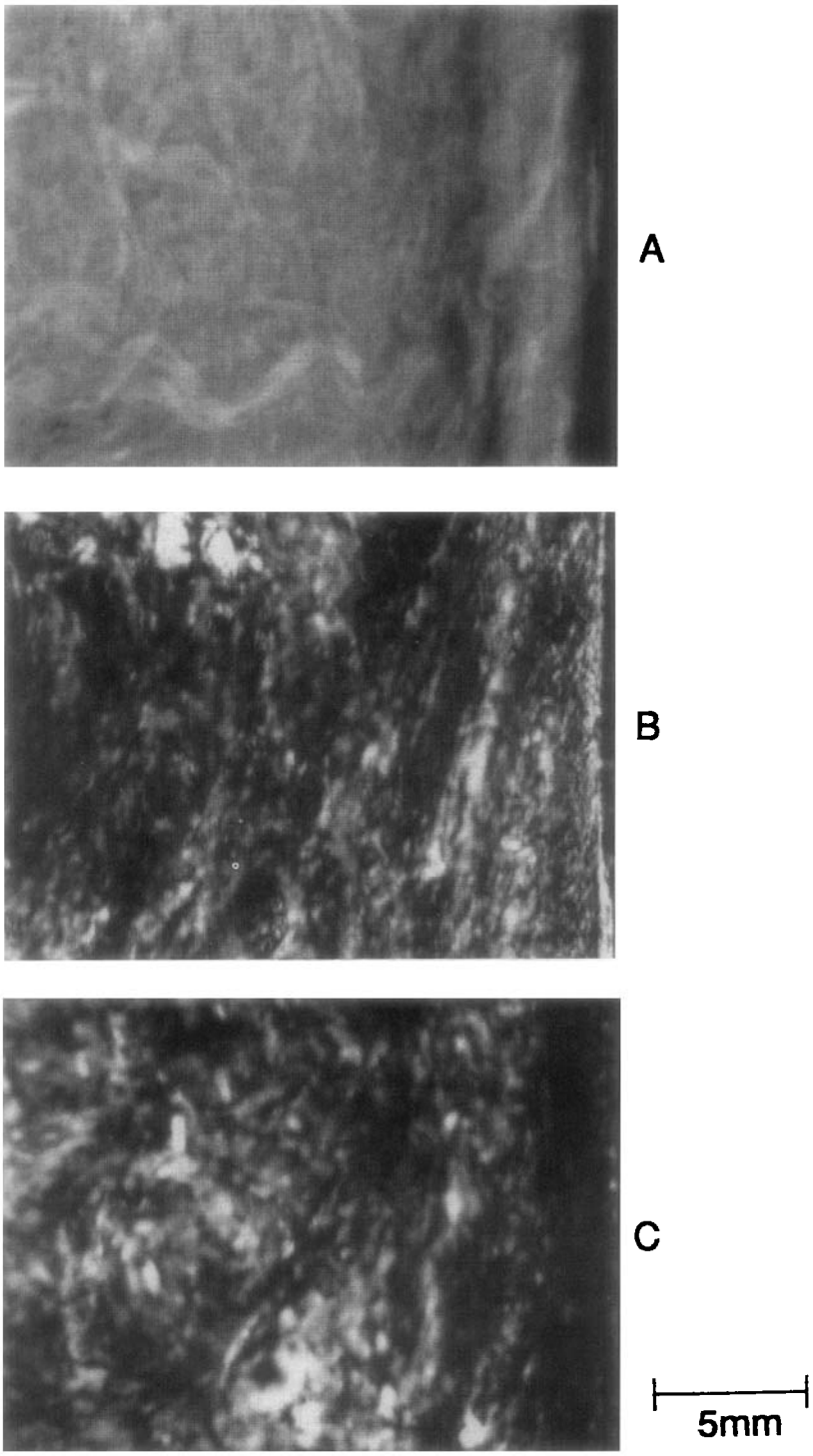

Figure 12 Three 30 MHz pulse mode images of a molding that was formed from an SMC with a proper flow front. The pulse mode images are from the (A) surface, (B) second, and (C) third groups of echoes.

images indicate that the acoustic signals did not penetrate to these depths but were reflected off an above discontinuity.

To verify if a large discontinuity was present in this region, an X–Z image was obtained from both the good and inferior moldings (Figs. 15 and 16, re-

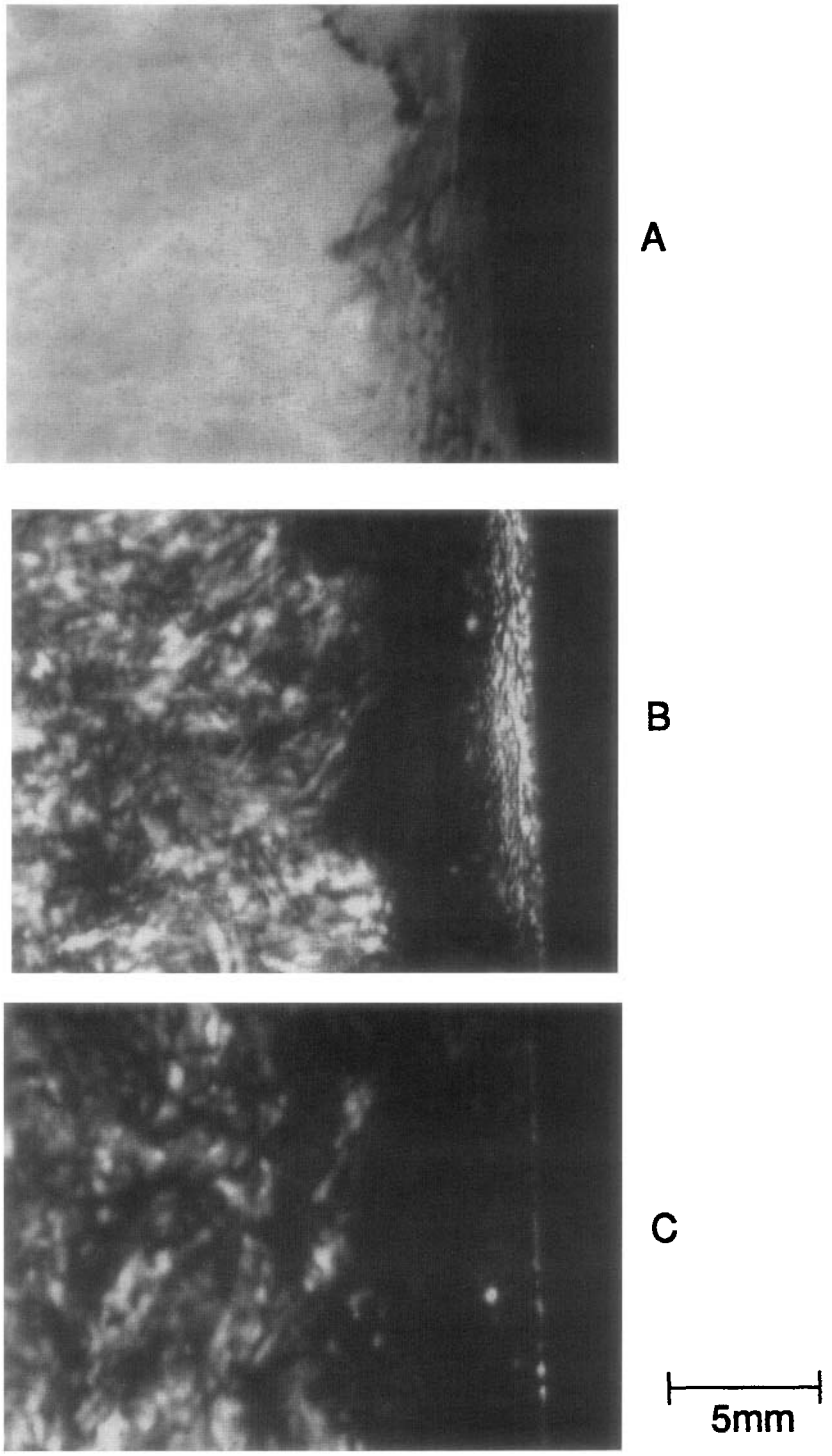

Figure 13 Three 30 MHz pulse mode images of a mold formed from an SMC that did not flow properly through an intricately-shaped die. The acoustic images are from the (A) surface, (B) second, and (C) third groups of echoes, respectively.

spectively). The *X-Z* image from the good mold [Fig. 15(B)] collected signals from the entire area below the surface. The two *X-Z* images from the inferior molding [Fig. 16(B) and (C)] indicate a large region below the surface where no acoustic signals were observed. Therefore, the *X-Z* images in-

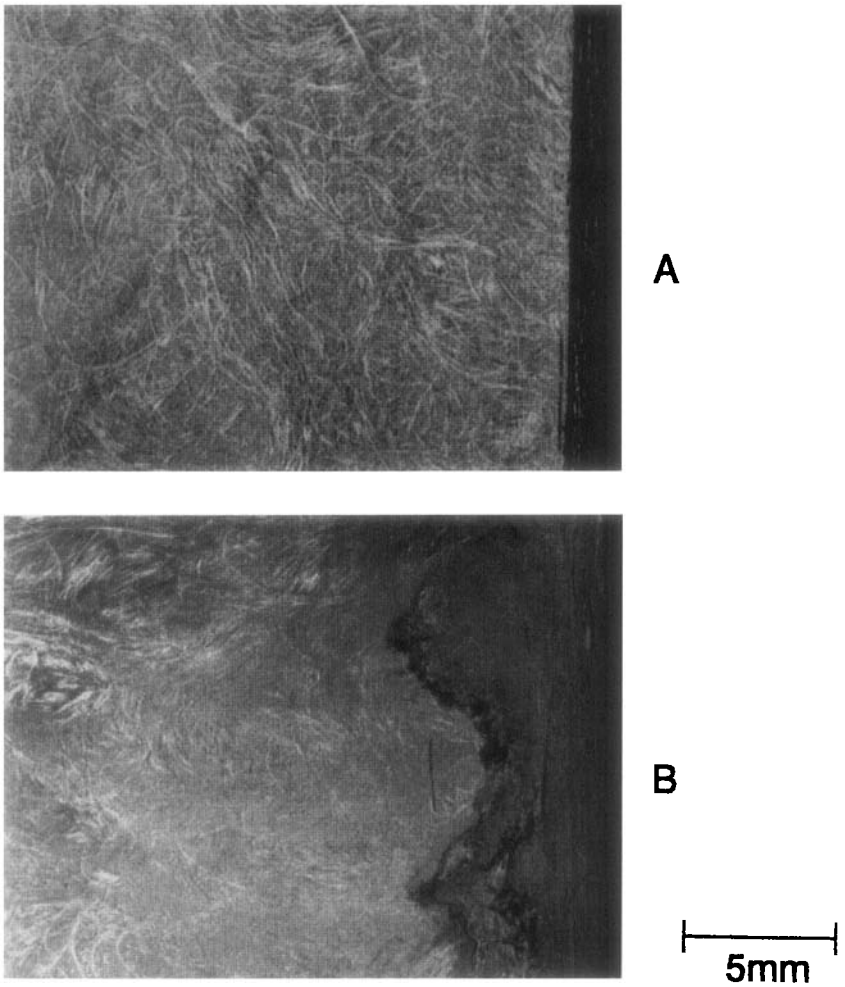

Figure 14 100 MHz pulse mode images from the surfaces of two moldings. (A) is from a molding with a proper flow pattern, whereas in (B), the SMC did not flow properly. The defect in (B) was detectable with the 100 MHz transducer because the defect was close to the surface.

dicate that a discontinuity is present directly below the surface that prevented the acoustic waves from penetrating into the sample. Note that the *X–Z* images show that the molded samples had a curved surface. In this case, the curvature did not dramatically affect the results of the pulse mode image. After reviewing the flow patterns, the discontinuity observed in the inferior molding was at a flow front. Hence, one can surmise that the resin cured prior to the intersection of the flow fronts, making the sample more susceptible to premature failure.

Burst Mode

Distribution of Chopped Fibers in PEEK

The orientation and distribution of the reinforcing material in any matrix is vital to the overall properties of the composite. Orientation and distribution of chopped carbon fibers in a PEEK matrix were investigated using the 600 MHz burst mode transducer. The composite was opaque, and the reflectivity of light from the matrix and fiber was similar; thus, the fibers were barely visible in the optical micrograph shown in Figure 17(A). However, the fiber and matrix differ drastically in their acoustic properties so that the reflected acoustic signals exhibit considerable contrast. Figure 17(B) shows the SAM image obtained from the reinforced composite. The variations in gray levels of the SAM images were attributed to differences in density and/or modulus. Since the two materials have sharply different moduli, the SAM images reveal the orientation and distribution of the fibers. The lighter areas at the end of a fiber indicate the portion of the fiber that was below the surface.

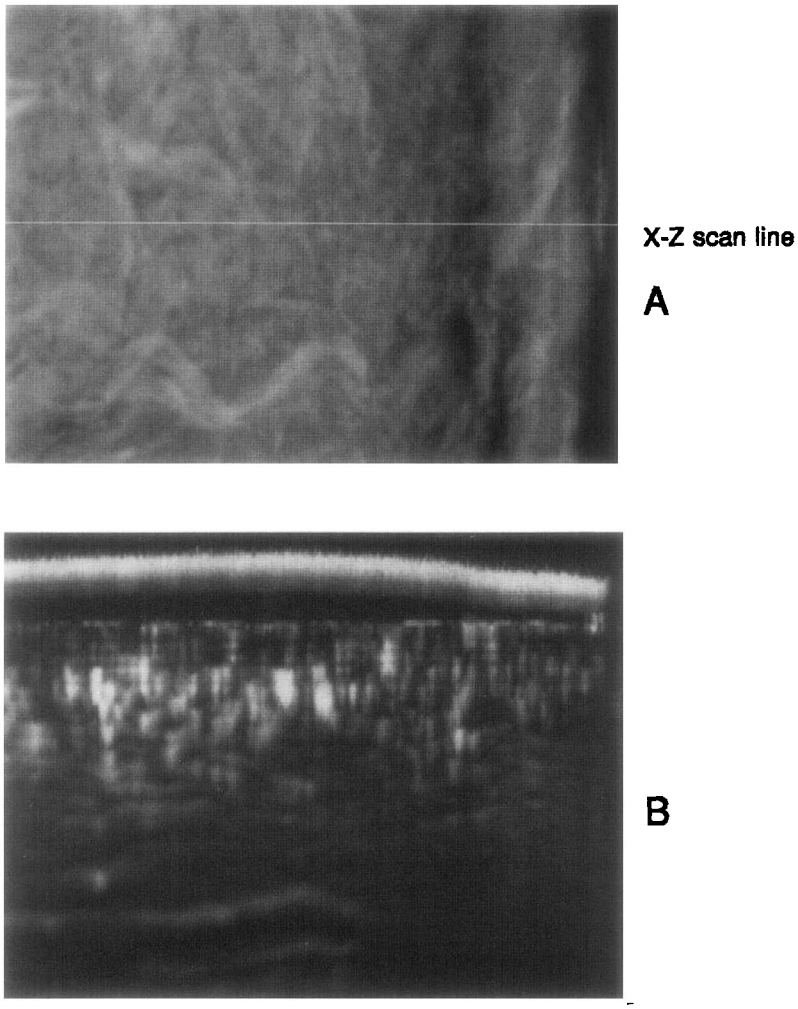

Figure 15 The *X-Z* image from the molding with a proper flow front. (A) shows the acoustic image from the surface echoes and the location of the *X-Z* line. (B) shows the acoustic signals below the surface in the *X-Z* image.

Carbon Black in an Elastomeric Matrix

Elastomeric materials, used as window sealants, contain submicron carbon black particles to increase the viscosity of the matrix adhesive. Both the processing history and the type of surfactant can be varied to increase the dispersion of the carbon black particles. The SAM was used to investigate the dispersion of the carbon black since the carbon black particles were not visible using conventional optical microscopy as shown in Figure 18(A). The imaging capabilities of the SAM cannot detect submicron particles, but can reveal the segregation and clustering of the carbon black particles. Traditionally, the carbon black distribution in the rubbery adhesive matrix is investigated by transmission electron microscopy. This technique will image the individual carbon black particles after many hours of tedious sample preparation. To investigate the dispersion of carbon black particles as it relates to the mechanical properties of the adhesive does not require imaging of the individual carbon black particles. Therefore, an acoustic microscope in the burst mode is well suited for this application.

Due to the low reflectivity of the adhesive, the reflected signal was too weak with the 600 MHz transducer, which prevented high-resolution images of the sample. Hence, the 200 MHz transducer was used to investigate the distribution of carbon black particles, though the resolution is much lower than the 600 MHz transducer used in the first burst mode example. The dispersion of carbon black particles with two process histories was investigated. The bright regions in the acoustic images in Figure 18(B) and (C) indicate clusters of carbon black particles, since these particles have a much greater stiffness

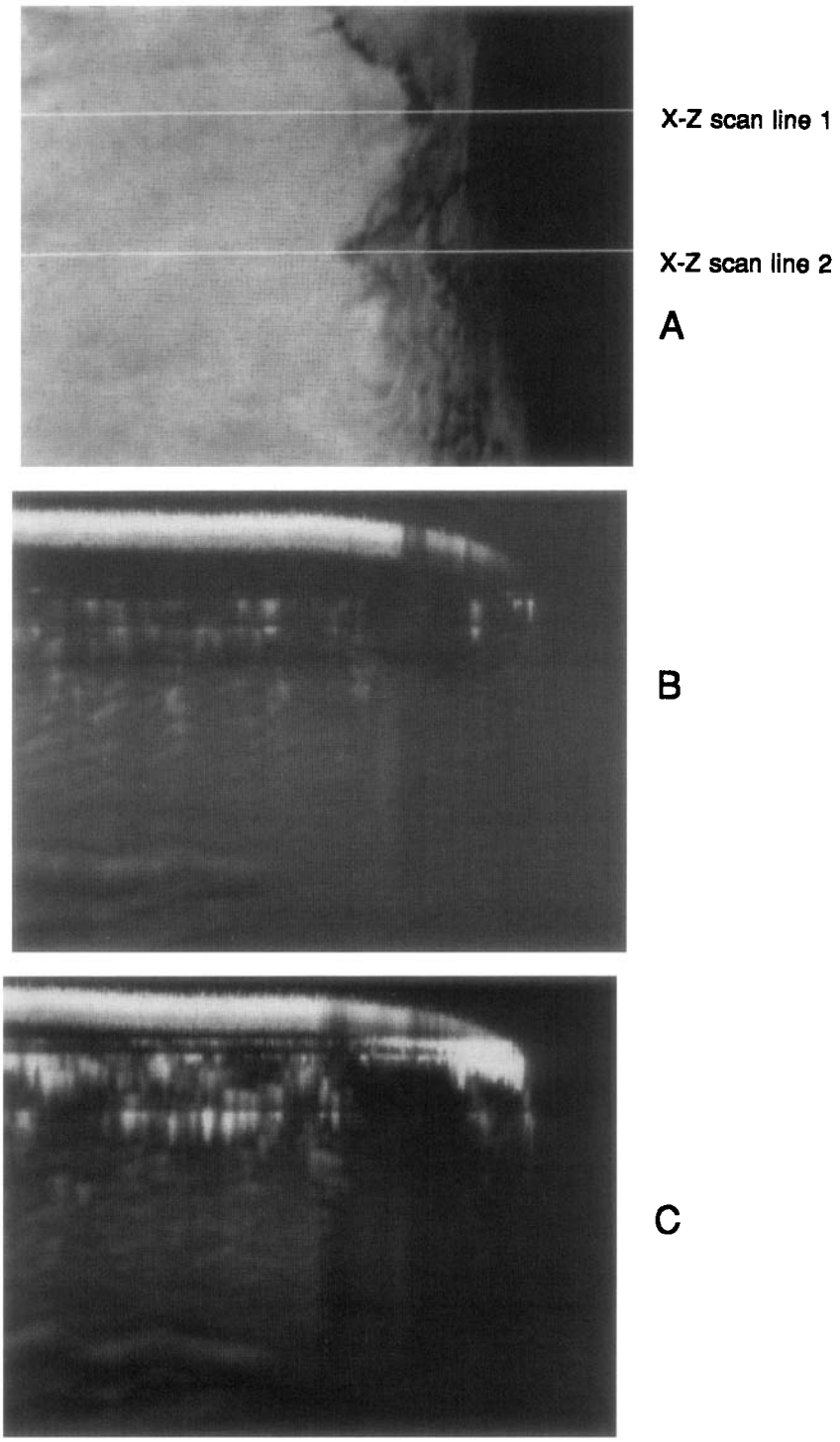

Figure 16 The *X–Z* image from the molding with an improper flow front. (A) shows the acoustic image from the surface echoes and the location of both of the *X–Z* lines. (B,C) show the acoustic signals below the surface in the *X–Z* images from the first and second lines, respectively. Notice the lack of echoes from beneath the defect.

than that of the elastomeric matrix. The burst mode image of the sample in Figure 18(B) reveals smaller clusters with uniform dispersion as compared to the sample in Figure 18(C). Hence, the dispersion of carbon black particles in the first sample was much more uniform throughout the matrix than in the

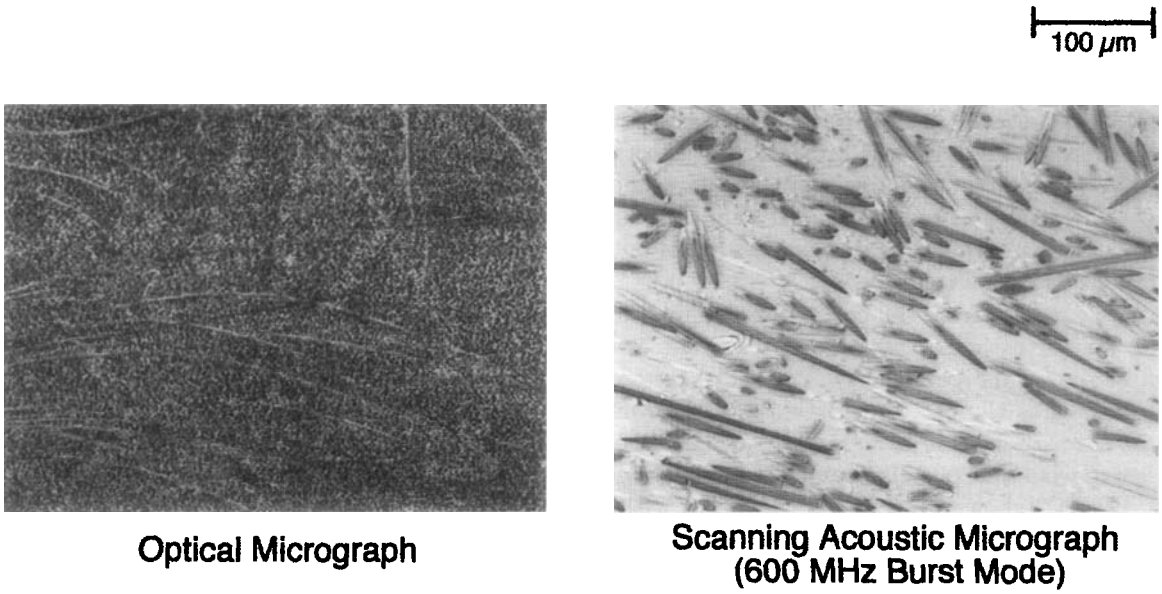

Figure 17 Comparison of the optical micrograph and scanning acoustic image of a composite with chopped carbon fibers in a PEEK matrix. (A) shows an optical micrograph of the composite, whereas (B) shows the acoustic image obtained with the 600 MHz burst mode transducer.

second case [Fig. 18(C)]. It was not surprising that there was a correlation of properties with dispersivity.

Orientation in Natural Biomaterials

Bone can be considered as a complex hierarchical composite of organic (collagen) and inorganic (hy-

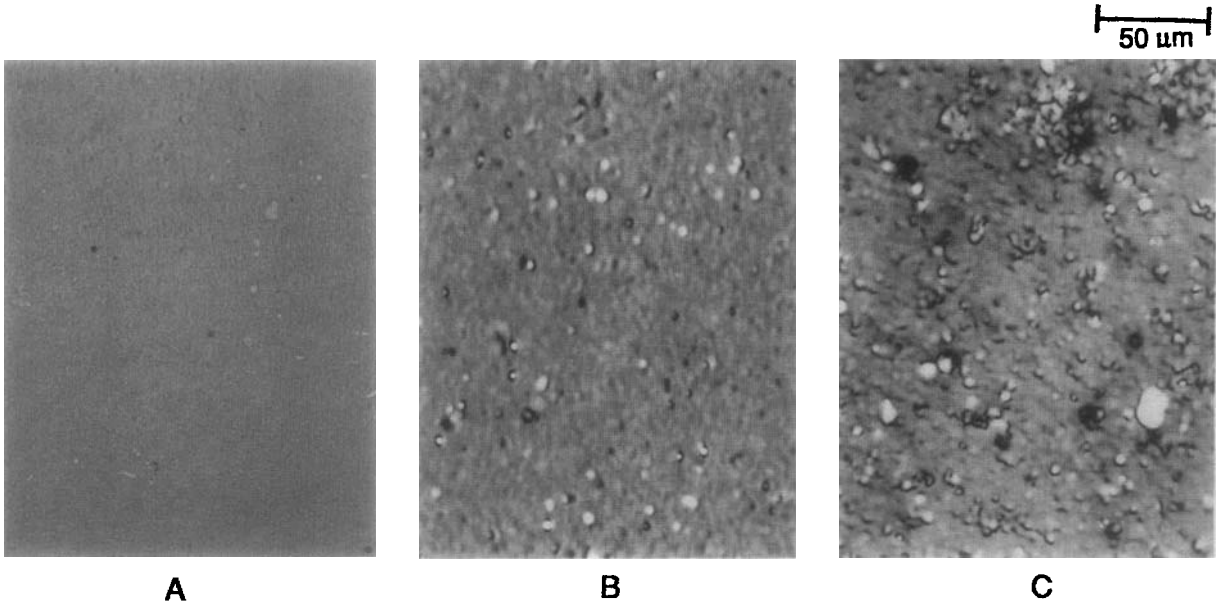

Figure 18 A comparison of the dispersion of carbon black in two adhesives prepared by different processes. (A) shows a typical optical micrograph of the adhesive. The carbon black particles appear white in the 200 MHz burst mode images because of their greater stiffness. The acoustic image from process A shows a good dispersion of carbon black particles (B), whereas the image from process B shows a poor distribution (C).

droxyapatite) components.[16] Traditionally, back-scattered electron microscopy has been employed to investigate the inorganic and organic regions in bone samples. Back-scattered electrons assess the density distribution of the inorganic mineral phase in the bone. The burst mode of the acoustic microscope detects differences in density as well as any change in local elastic properties due to orientation of both the mineral and collagen phases.

A single osteon from the cortical region of a dog femur was investigated with back-scattered electrons, as shown in Figure 19(A). The back-scattered image indicates the osteon is essentially the same density throughout. The same osteon, which was investigated with the 600 MHz burst mode transducer [Fig. 19(B)], showed a lamellar structure within the osteon. Thus, acoustic microscopy is capable of identifying various orientations of the mineral phase within the osteon. In essence, the back-scattered electron microscope image verifies the density gradients within a material. However, the acoustic microscope can complement this analysis by identifying the orientation of the respective lamellae in the osteon.

The ability of the SAM to image variations in orientation has also been used for investigation of collagen fibers in a sheep meniscus.[17] The large variations of the acoustic signal from various orientations of collagen fibers were obtained with a 400 MHz burst mode transducer (Fig. 20). The SAM image provides details in the orientation of the collagen fibers in the meniscus that normally would not be observed without applying a biological stain. In fact, the SAM image is very similar to an optical micrograph of a stained meniscus.

Multilayer Polymeric Composites

A coextruded microlayer composite composed of alternating layers of polycarbonate (PC) and styrene–acrylonitrile copolymer (SAN) exhibited improved mechanical properties such as toughness and ductility.[18] The failure processes of the 49-layer composite with a PC-to-SAN ratio of 26/74 was investigated with a minitensile stage mounted on the SAM stage. The SAM was used to investigate the failure mechanisms as well as the interfaces between the layers.

The 400 MHz transducer obtained an image from the composite after it was elongated 9.75%. The SAM image [Fig. 21(A)] showed the initial stage of craze formation in the SAN layers. This image was slightly better quality than the optical micrograph shown in Figure 21(B). Software features as-

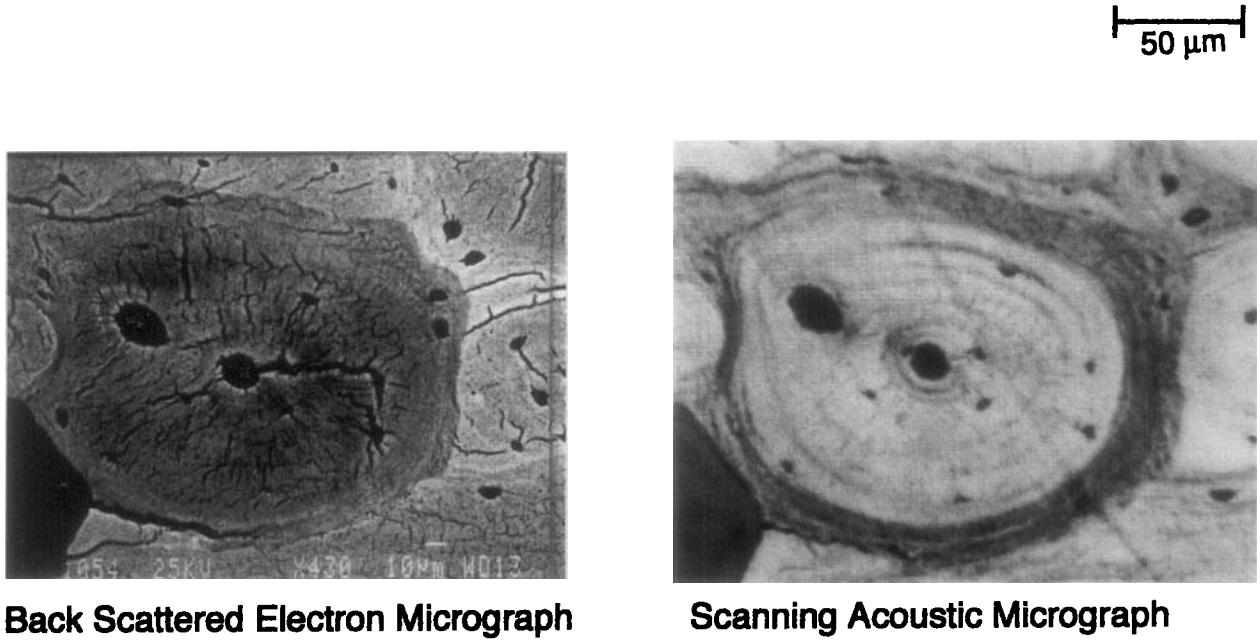

Figure 19 An example of how scanning acoustic microscopy can complement back-scattered electron microscopy using a single osteon from the cortical area of a dog femur. The back-scattered electron micrograph in (A) showed areas with similar mineral densities. The 600 MHz burst mode transducer provided variations in orientation of the mineral phase (B).

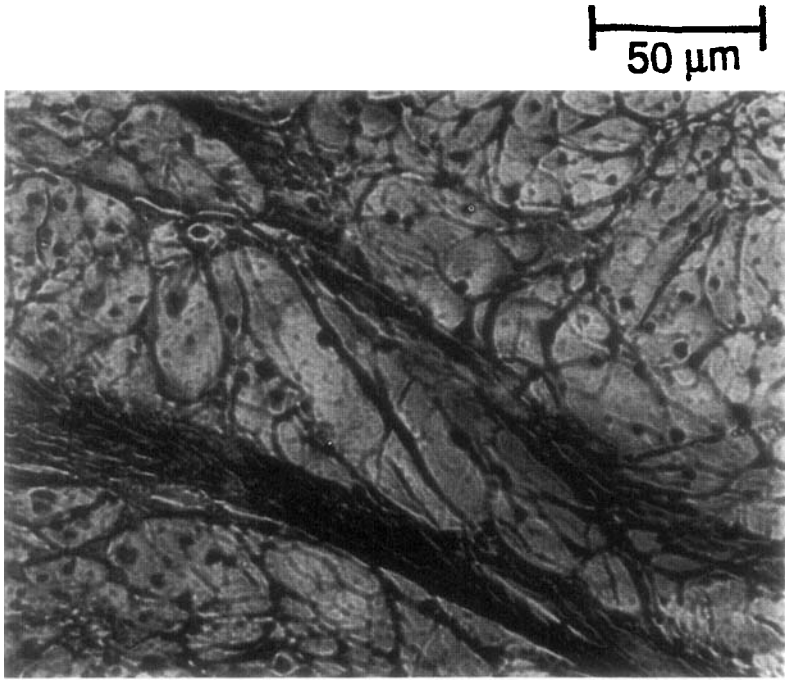

Figure 20 The 400 MHz burst mode image of a sheep's meniscus composed of collagen fibers. The variations in gray levels are a result of different orientations of the collagen fibers.

sociated with the SAM are also capable of manipulating the 2-dimensional surface image to provide a pseudo-3-dimensional representation of the surface image (Fig. 22). SAM showed that the SAN layers were slightly higher than the PC layers after polishing.

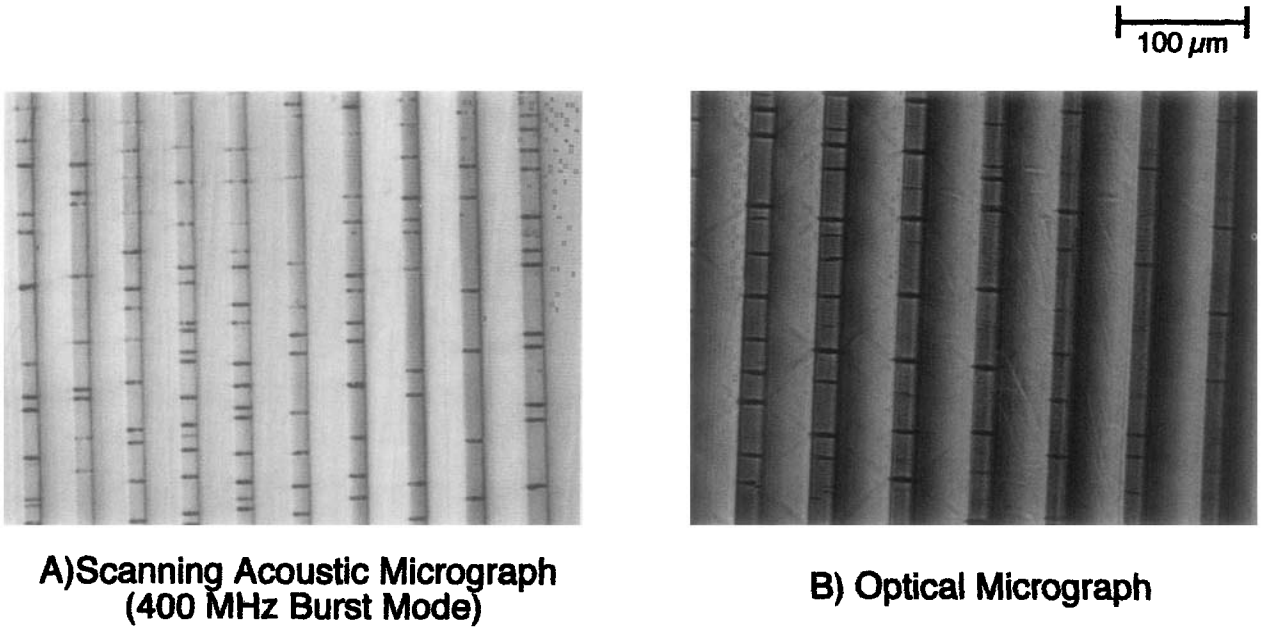

Figure 21 A comparison of the optical micrograph and acoustic image of a coextruded microlayer composite composed of alternating layers of PC and SAN with a ratio of PC/SAN of 26/74. (A) is a 400 MHz image of the multilayer composite after it was elongated 9.75%. (B) shows the corresponding optical micrograph.

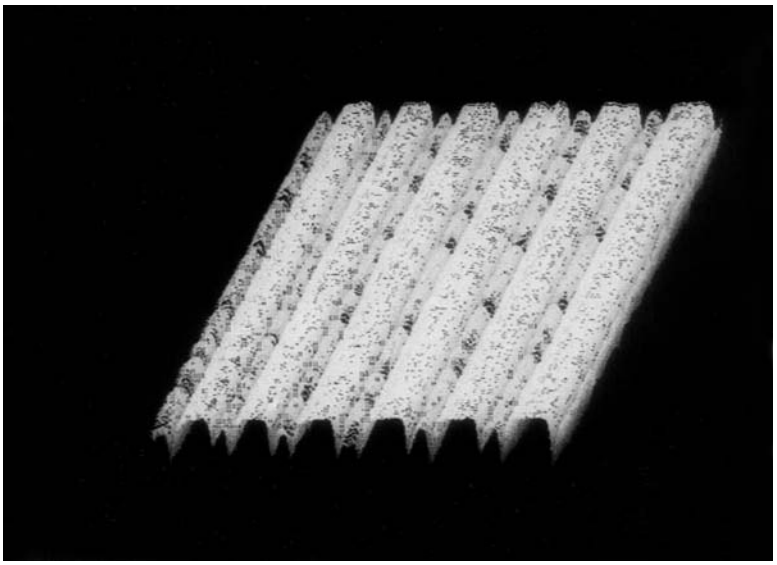

Figure 22 A pseudo-3-dimensional acoustic microscopy image of the coextruded microlayer composite's surface. The 3-dimensional image was created from the gray level intensities of the 2-dimensional image in Figure 21(A).

Particle–Particle Interaction of PET in PVC/MBS Blend

Small amounts of PET existing in recycled PVC can adversely affect the properties of the reprocessed PVC resin.[19] PET does not melt during proc and exists as rigid particulate inclusions in th system. SAM was used to study the failure pr during uniaxial tensile deformation of th

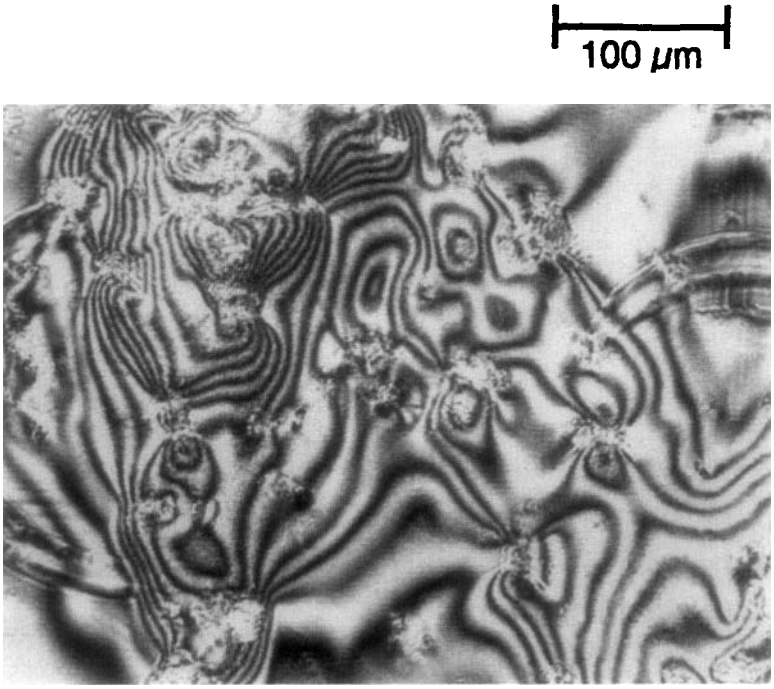

Figure 23 The 200 MHz burst mode image of a PVC matrix filled with PET. The strain fields around the PET particles were detected when the transducer was defocused ($z = -100\ \mu m$).

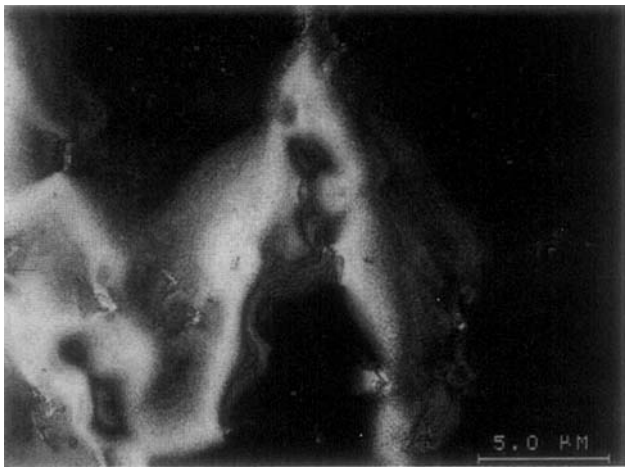

A: First Echo

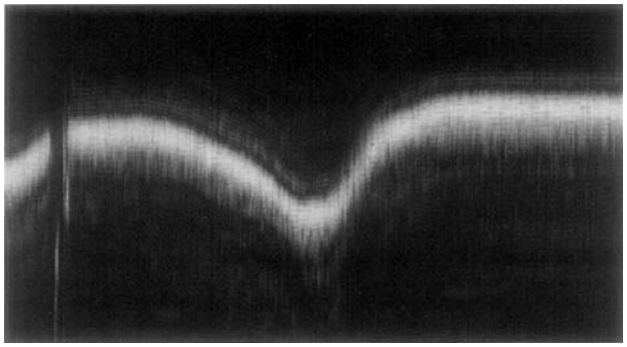

B: First X-Z image

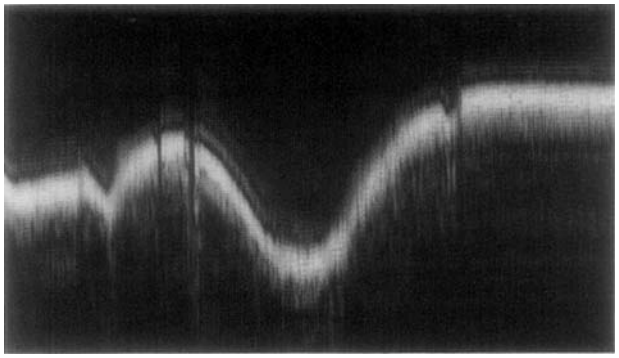

C: Second X-Z image

Figure 24 A PVC blend filled with PET particles. (A) shows the SAM image from the surface using the 200 MHz transducer, with the location of both X-Z scans. (B,C) show the X-Z scans corresponding to the first and second scans in (A). The X-Z scans show a deflection in the acoustic signal on the surface that was used to calculate the thickness reduction.

blend filled with 5% PET. The minitensile apparatus was mounted on the SAM stage so that the sample could be examined with 6% applied strain.

The 200 MHz burst mode transducer obtained images of strain fields around the particles in the PVC matrix, as shown in Figure 23. The strain applied to the specimen caused topographical changes of the surface. Hence, a lower-frequency transducer

with a larger focal point was required to investigate the changes in thickness caused by the stress concentrator. Optically, this region would have appeared as a stress-whitened zone. The thickness reduction in this highly plastically deformed range was measured in two different zones using an X–Z image. As the transducer was lowered, the acoustic echoes were collected from the changing topography, as shown in Figure 24. At 6% strain, the total thickness reduction in the stress-whitened region was approximately 30% of the original thickness.

CONCLUSIONS

Both the pulse and burst operating modes in scanning acoustic microscopy have been successfully used to investigate nondestructively a large variety of mostly opaque polymeric materials and composites. These modes complement each other in the analysis of different features within the material. The pulse mode was used mainly for deep internal examination but with lower resolution. Internal damage caused by impact in oriented polypropylene and two carbon fiber-reinforced composites was observed. Also, the flow paths of chopped glass fibers and an internal defect resulting from various flow fronts were revealed with the pulse mode.

The burst mode was used to analyze the surface and subsurface features of materials with higher resolution. The dispersivity of carbon black particulates and chopped carbon fibers in polymeric matrices was studied. Together with light and electron microscope techniques, the unique ability of the burst mode to characterize differences in moduli was employed to investigate the orientation and density differences in the lamellar structure of a single osteon from a dog femur and the orientation of collagen in a meniscus from a sheep. Finally, the burst mode was used to investigate the surface relief of a multilayer composite caused by polishing and the topographical change in a PVC matrix due to elongation.

With these examples, it was demonstrated that scanning acoustic microscopy will become a major technique for nondestructive examination particularly of opaque systems, thus complementing electron and optical microscopy.

The authors would like to thank the NASA Center for Commercial Development of Space on Materials for Space Structures (CMSS), the Center for Applied Polymer Research (CAPRI), the Edison Polymer Innovation Corp. (EPIC), the National Science Foundation (NSF), and the Army Research Office Durham (AROD) for their financial support.

REFERENCES

1. L. W. Kessler and D. E. Yuhas, *Scan. Elect. Microsc.*, **1**, 555 (1978).
2. R. A. Lemons and C. F. Quate, *Appl. Phys. Lett.*, **24**, 163 (1974).
3. C. F. Quate, A. Atalar, and H. K. Wickramasinghe, *Proc. IEEE*, **67**, 1092–1114 (1979).
4. G. A. D. Briggs, *Acoustic Microscopy*, Clarendon Press, Oxford, 1992.
5. R. G. Wilson and R. D. Weiglein, *J. Appl. Phys.*, **55**(9), 3261–3275 (1984).
6. B. Derby, G. A. D. Briggs, and E. R. Wallach, *J. Mater. Sci.*, **18**, 2345–2353 (1983).
7. D. G. P. Fatkin, C. B. Scruby, and G. A. D. Briggs, *J. Mater. Sci.*, **24**, 23–40 (1989).
8. M. G. Somekh, G. A. D. Briggs, and C. Ilett, *Philos. Mag.*, **49**(2), 179–204 (1984).
9. K. Fossheim, T. Bye, S. Sathish, and G. Heggum, *J. Mater. Sci.*, **23**, 1748–1751 (1988).
10. I. Ishikawa, T. Semba, H. Kanda, K. Katakura, Y. Tani, and H. Sato, *IEEE Trans. Ultrason. Ferroelect. Frequency Control*, **36**(2), 274–279 (1989).
11. K. Yamanaka, Y. Enomoto, and Y. Tsuya, *IEEE Trans. Sonics Ultrason.*, **SU-32**(2), 313–319 (1985).
12. Q. R. Yin, C. Ilett, and G. A. D. Briggs, *J. Mater. Sci.*, **17**, 2449–2452 (1982).
13. K. Yamanaka and Y. Enomoto, *J. Appl. Phys.*, **53**(2), 846–850 (1982).
14. A. Quinten and W. Arnold, *Mater. Sci. Eng.*, **A122**, 15–19 (1989).
15. S. J. Pan, H. R. Brown, A. Hiltner, and E. Baer, *Polym. Eng. Sci.*, **26**(14), 997–1014 (1986).
16. A. Meunier, O. Riot, J. L. Katz, P. Christel, and L. Sedel, in *IEEE 1989 Ultrasonic Symposium*, IEEE, New York, 1989, pp. 1015–1018.
17. A. Meunier, J. L. Katz, P. Christel, and L. Sedel, *J. Orthop. Res.*, **6**, 770–775 (1988).
18. B. L. Gregory, A. Siegmann, J. Im, A. Hiltner, and E. Baer, *J. Mater. Sci.*, **22**, 532–538 (1987).
19. J. Li, M. Twigg, A. Hiltner, and E. Baer, **52**, 285 (1994).

Received March 4, 1993
Accepted June 10, 1993